DIPSI Workshop 2011 on Droplet Impact Phenomena & Spray Investigation
May 27, 2011, Bergamo, Italy

EXPERIMENTAL AND NUMERICAL CHARACTERIZATION OF HIGH-PRESSURE SPRAYS FOR GDI ENGINES

L. Allocca (*), A. Montanaro (*), T. Lucchini (°), F. Brusiani (†)

(*) Istituto Motori CNR - Napoli, Italy
(°) Politecnico di Milano - Dipartimento di Energia, Italy
(†) Università degli Studi di Bologna, Italy

ABSTRACT

Direct-injection is now widely applied in spark-ignition engines in combination with turbocharging to reduce the fuel-consumption and the knock risks. This is achieved through the use of multi-hole, high-pressure injectors whose features are rather different with respect to the hollow-cone, low-pressure configurations that were adopted in the last decade. This last aspect has to be taken into account when multi-dimensional simulations of GDI engines have to be performed. In particular, suitable models are needed to describe the spray atomization and the wall-impingement processes.

In this paper experimental investigations were performed using a 6-hole injector in a constant-volume vessel with optical access. Spray images were acquired by a CCD camera and processed to obtain the spray penetration and cone angles for the different tested operating conditions. The effects of injection pressure were evaluated in the range 3.0 – 20 MPa at ambient density of the gas. A flat plate was added to the experimental apparatus for investigation of the spray-wall impingement and liquid-film images were acquired. On the basis of the experimental database, a CFD methodology for gasoline spray simulations was implemented into the Lib-ICE code, developed under the OpenFOAM technology. The evolution of the resulting liquid film was also taken into account by solving the mass and momentum equations on the mesh boundary.

INTRODUCTION

In the field of SI-engines, attention is mainly focused on Direct Injection (GDI) because it allows to improve the overall engine thermal efficiency and the engine response during load variations. A significant reduction of the knock tendency is also ensured and this is a relevant aspect when turbocharging is used [1, 2]. GDI technology allows the reduction of HC and CO emissions especially at cold start (warm-up period) and transient modes when the engine works at lean-mixture conditions. To take advantage of all the theoretical benefits derived from GDI applications, it is necessary to work with a large stratification region in the engine map and this requires a strong control of the air/fuel mixing process.

The most widely used GDI injector configuration is the multi-hole mini-sac injector which is used to deliver fuel during the intake and compression strokes, with pressures ranging from 1 to 20 MPa [3]. The fuel/air mixture distribution is the result of complex interactions between the emerging fuel spray, in-cylinder flow field and the combustion chamber geometry [4]. Hence, experimental and numerical investigations are needed to evaluate how the spray evolution is influenced by nozzle design and spray targeting [5], injection pressure [6] and the interaction between spray and cylinder/piston walls [7].

In particular, multi-dimensional models are widely applied to real engine geometries to define suitable injector configurations and strategies for a wide range of operating conditions. The well-known Eulerian-Lagrangian approach is used to model the fuel spray, which is composed by a discrete set of computational parcels and their evolution depends on the exchange of mass, momentum and energy with the continuous gas phase. Additional sub-models are also required to take into account the liquid jet atomization, droplet evaporation, heat transfer, breakup, collision and wall impingement [8].

In this work, experiments and calculations were performed to understand the behavior of a gasoline spray emerging from a six-hole injector mounted on the top of an optically accessible vessel. This investigation was performed to provide a reliable CFD methodology to simulate these jets. Different injection pressures were considered, ranging from 3 to 20 MPa and the injected mass flow rate was measured for each operating conditions. A CCD camera was used to acquire the spray images that were then digitally processed to measure the spray penetration and cone angles. Impinging conditions were also reproduced in the experiments by introducing a plate in the vessel orthogonally oriented with respect to a reference jet.

The proposed CFD approach was implemented by the authors into the Lib-ICE code [9, 10], which is a set of libraries and applications for engine modeling developed under the OpenFOAM® technology [11]. Specific modules are available for the simulation in in-cylinder processes (Diesel and HCCI combustion, motion of piston and valves, complex chemistry with adaptive tabulation, gas and particulate emissions, spray break-up and spray-wall interaction). In previous works, Lib-ICE was applied to simulate the fuel-air mixing process in Diesel and PFI engines [12, 13]. A simplified 1-D model of the nozzle flow was used to estimate the influence of cavitation on the liquid jet diameter and velocity while the primary and secondary liquid jet break-up processes were modeled according to the Kelvin-

(*) corresponding author: l.allocca@im.cnr.it – tel +39 081 7177152 – fax +39 081 2396097

Helmoltz theory. A specific spray sub-model describes the interaction between the fuel spray and the cylinder walls under different impinging conditions and the evolution of the resulting liquid film is also taken into account by solving its mass, momentum and energy equations on the mesh boundary.

EXPERIMENTAL APPARATUS

The GDI injector considered in the present work was the mini-sac six-holes Bosch HDEV 5.1 with solenoid actuation. This injector is characterized by a hole diameter of 0.193 mm and a range of application between 5.13 and 17.1 g/s of delivered fuel for an injection pressure of 10 MPa. On a plane perpendicular to the injector axis, the six jet directions give a spray footprint characterized by a hollow-ellipsoid shape.

To avoid interference and contamination with the surrounding ambient, the fuel was discharged from the injector into a quiescent vessel filled with air kept at atmospheric pressure (0.1 MPa) and room temperature. The high pressure for the injections was generated by a hydro-pneumatic pump, instead of the classic rotating pump, activated by pressured gas (air) ranging from 0.07 MPa to 0.7 MPa. The injector was driven by a Programmable Electronic Control Unit (PECU) able to manage multi-injection strategies with the needle opening time defined through the injector energizing period. The injection flow rate was measured by an AVL Meter operating on the Bosch principle [14,15]. During the experimental tests the injection pressure range from 3 MPa to 20 MPa was considered and it corresponded to a delivered fuel quantity ranging between 10 and 100 mg/stroke.

During the experiments, pictures of the emerging spray were taken using a synchronized CCD camera characterized by 1376x1040 pixels, 12 bit resolution, and 0.5 μs shutter time. A wet seal spherical holder enabled the tilting of the injector in an angular range of +/- 15°, with respect to its axis. It allowed the perpendicular alignment between the direction of one spray and the CCD optical axis, therefore the parallax error was reduced. The spray pictures were taken at different instants starting from SOI and they were post-processed by software to extract the main parameters characterizing the dynamic of the spray: cone angle and liquid penetration. In particular, these quantities were measured only on one of the six jets emerging from the injector. At this scope the jet characterized by the smallest interactions with the other jets was chosen. More details about image post-processing procedure can be found in [16].

Finally, a stainless steel flat plate was introduced into the vessel to reproduce the spray-wall impingement. The plate was located at 40 mm from the nozzle tip thanks to a X-Y-Φ micrometric apparatus. The plate axis was parallel the axis of the less interacting jet, fully framed by the CCD camera. The plate was at same room temperature of the gas filling the vessel. The authors decided to perform also spray impact analysis because, as well known, for GDI engines the wall film liquid formation on the combustion chamber walls during the compression strokes could be a very significant problem because it has a strong influence on the air/fuel mixing process, therefore on the combustion performance and pollutant formation. For this reason a correct prediction of wall film (generation and evolution) is of great importance for GDI engine simulations. For all the experimental tests, a standard (commercial) gasoline was used as fuel.

NUMERICAL MODELS

The modeling requirements that have to be satisfied to perform a spray simulation are quite high because during the injection the jets outgoing the injector nozzles are simultaneously subjected to many phenomena: primary atomization, secondary break-up, collision/coalescence and wall-impingement. In the following sections, the spray sub-models implemented in the Lib-ICE code are presented.

Breakup model

To define the droplet velocity components at nozzle exits, the Huh-Gosman [17] theory was considered. A quasi-dimensional turbulence model was used to compute the turbulent kinetic energy (k_{d0}) and dissipation rate (ε_{d0}) of the emerging liquid jet, which were initialized according to the flow conditions inside the nozzle:

$$k_{d0} = \frac{U_D^2}{8L_{nozz}/D_{nozz}}\left[\frac{1}{C_d^2} - K_c - (1-s^2)\right] \qquad (1)$$

$$\varepsilon_{d0} = K_\varepsilon \frac{U_D^3}{2L_{nozz}}\left[\frac{1}{C_d^2} - K_c - (1-s^2)\right] \qquad (2)$$

where C_d is the discharge coefficient and K_c - K_ε are two model constants respectively set to 0.47 and 0.23. L_{noz} and D_{noz} are the geometric length and diameter of the injector nozzle. U_d is the droplet velocity at nozzle exit and s the area ratio at the contraction corner.

From k_{d0} and ε_{d0} it was possible to estimate the turbulent length and time scales L_{t0} and τ_{t0} at the time the blob leaves the nozzle:

$$L_{t0} = C_\mu \frac{k_{d0}^{1.5}}{\varepsilon_{d0}}, \tau_{t0} = C_\mu \frac{k_{d0}}{\varepsilon_{d0}} \qquad (3)$$

C_μ is a constant whose value is equal to 0.09. The spray cone angle, α, is then estimated as:

$$\tan\left(\frac{\alpha}{2}\right) = \frac{C_1 \cdot L_{t0}}{C_3 \cdot \tau_{t0}} \qquad (4)$$

Where the values of the model constants C_1 and C_3 were set to 2.0 and 1.2 respectively [17].

Since the injection pressure in GDI engines usually ranges from 5 MPa to 20 MPa, the resulting droplet Weber number at the nozzle exit is generally lower than 1000, which was fixed as threshold between turbulence-induced and aerodynamic-induced breakup [12, 18]. For this reason, the Kelvin-Helmoltz instability was chosen to be the dominant mechanism governing both the primary and secondary droplet break-up [19]. The diameter reduction of the injected blobs was computed as:

$$\frac{dD_d}{dt} = -\frac{D_d - D_{new}}{\tau_{BU}} \quad (5)$$

where D_d is the current droplet diameter, D_{new} is the diameter of the child drops and τ_{BU} is the break-up time. These values were computed according to the most unstable growth rate Ω and wavelength Λ:

$$D_{new} = 1.22 \cdot \Lambda \quad (6)$$

$$\tau_{BU} = 3.788 \cdot B_1 \cdot \frac{D_d}{2 \cdot \Lambda \cdot \Omega} \quad (7)$$

where B_1 is a tuning constant, which was set to 6 in this work. The reader is referred to [19, 20] for further details about the Kelvin-Helmoltz breakup model and the calculation of the wavelength and the growth rate.

As well known, high pressure GDI injectors are generally affected by cavitation. In a previous work, the authors studied the cavitation phenomena into a six-hole GDI injector very similar to that considered in the present analysis [21].

Collision model

To model collision in this work, the Nordin approach was adopted [8]. It states that collision between two parcels occurs only if, in the same integration step, their trajectories intersect and the intersection point is reached at the same time. This condition is fulfilled only when two parcels are travelling towards each other and their relative distance is greater than their size. The model accounts for both stretching separation and coalescence [22]. The Nordin model presents a reduced grid-dependency and this aspect is rather important when spray is simulated in unstructured and deforming meshes [8].

Wall-Impingement model

The interaction between the spray parcels and the liquid film is modeled with the approach proposed by Stanton et al. [23]. Generally, the collision between a drop and a wet surface may result in four different regimes: sticking, spreading, rebounding and splashing [24].

The impingement regimes are identified by the Weber number *We* defined as:

$$We = \frac{\rho \cdot V_p \cdot N_w \cdot d_0}{\sigma} \quad (16)$$

Where $\mathbf{V}_P$ is the relative velocity between the droplet and the wall, $\mathbf{n}_w$ is the face normal of the impinging wall, d_0 the droplet diameter and σ is the surface tension. The following transition criteria were used:

- We < 5 : stick
- 5 < We < 10 : rebound
- 10 < We < We_S : spread
- We > We_S : splash

W_{es} represents the splashing threshold and is given by [25, 26]:

$$We_S = 18^2 d_0 \left(\frac{\rho}{\sigma}\right)^{1/3} \left(\frac{\mu}{\rho}\right)^{1/4} f^{3/4} \quad (17)$$

where ρ, σ, μ, d_0, and f are the drop density, surface tension, dynamic viscosity, incident drop diameter, and frequency of drops impinging on the film.

The splashing process is modeled by introducing three new parcels in the mesh for each impinging droplet. A detailed description of the correlations used for momentum and mass exchange between the droplets and the liquid film in the rebound and splash regimes can be found in [25, 26].

Liquid-Film model

The formation of the liquid film is the result of the interaction between the injected fuel spray and the computational domain walls. For an engine simulation, a good prediction of the liquid film generation and evolution is mandatory because it has a strong influence on the fuel-air mixing process. In the paper, to simulate the wall film a shallow water formulation was adopted for the flow equations, solving for mean thickness, momentum and energy in a conservative manner. The liquid film equations were discretized on a curved 2-D surface in 3-D, accounting for its curvature and motion using the Finite Area Method. Faces of arbitrary shapes are supported, therefore it can be used with complex geometries like IC engines [13].

Adaptive local mesh refinement (ALMR)

ALMR enables a high mesh resolution where the fuel air mixing process takes place, while the overall grid size is weakly increased. The proposed approach works with hexahedral moving meshes. An initial computational mesh has to be provided by the user, whose size should be fine enough to correctly reproduce the geometrical domain to be simulated and the main details of the initial flow-field. Following previous approaches [27, 28], a geometric field is chosen as an error estimator and when its values lie in a user-specified interval the parent cell is split into eight child cells by introducing new nodes at the cell centroid and at the mesh face centers [29]. An arbitrary level of refinements can be chosen by the user as well as a maximum number of cells to control the mesh size. Grid un-refinement is also possible when the values of the error estimator are outside the specified interval. The geometric field used as a refinement criterion is represented by the total fuel mass fraction (liquid and gas) in each cell:

$$Y_{l+g} = \frac{m_{f,l} + \rho \cdot Y_f \cdot V_{cell}}{\rho \cdot V_{cell}} \quad (21)$$

where m_{fl} is liquid mass of all the parcels belonging to the cell, Y_f is the fuel mass fraction in the gas phase, ρ is the gas phase density, and V_{cell} is the cell volume. The consistency of the ALMR approach was verified in previous works for both evaporating and non-evaporating spray [12, 30]. It was shown

that, depending on the chosen level of refinements, ALMR provides the same results of a uniform fixed mesh with the same minimum size. The comparison was performed in terms of spray penetrations and equivalence ratio distribution at different distances from the injector.

RESULTS AND DISCUSSION

Experimentally, different injection strategies were tested changing the injection duration, the injection pressure and the total injected mass. All the investigated configurations are collected in Table 1. At constant injection pressure, the injected fuel mass was increased by operating on the electric pulse duration. For each configuration, the injected fuel mass measured by the AVL Meter was compared with the weighted ones obtained by using a precision balance. The discrepancies were always lower than 2%. For each configuration reported in Table 1, the fuel injection rate was extracted from the experiments as the average of one hundred of shots. For example, Figure 1 shows the injection profiles obtained for mass fuel injected equal to 20 and 50 mg/stroke. It is interesting to note as all the profiles were quite similar in the overlapping parts.

Table 1: Time durations of the pulses for the desired fuel amounts at the indicated injection pressures.

t_{inj} [ms]		Total Injected Fuel Mass [mg/stroke]			
		10	20	50	100
P_{inj} [MPa]	3	1,3			
	6	0,9			
	10		1,45	3,6	
	15			2,9	5,8
	20			2,6	5,1

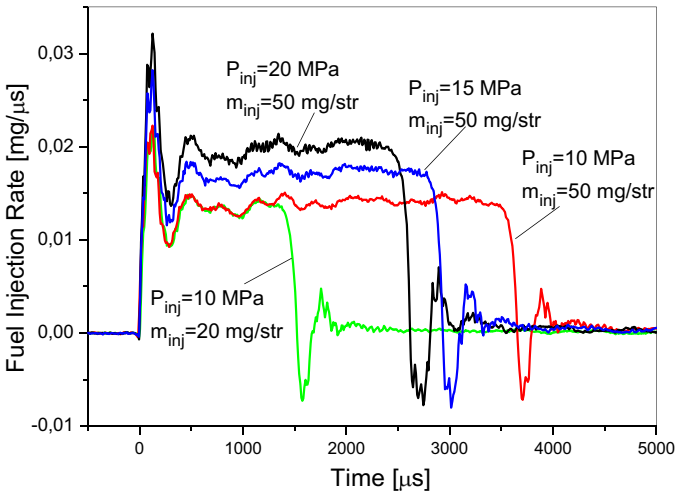

Figure 1: Profiles of the fuel injection rate for different injection conditions.

The evolution of the spray inside the vessel was monitored by the CCD camera synchronized with a flash light. A suitable spatial injector orientation enabled a full view of one of the six injector sprays. The CCD shutter, synchronized with the spray command at different instant from the start of the injection, limited image blurring and time indetermination to 0.5 μs.

Observing the spray from the lateral view, it was possible to evaluate the spray structure evolution and, in particular, the evolution of the interaction between the different jets. For example, Figure 2 shows the spray evolution recorded for the case: P_{inj}=20 MPa and m_{inj}=50 mg/stroke. As showed, during the first injection part the interaction between the jets was almost negligible. At later time (injection time higher than 400 μs) the jet swellings became evident and fuel pockets were generated by the coalescence phenomena. They were clearly visible by the experimental pictures because highlighted by the highest intensity in the scattered light. This was an unambiguous sign of a non-homogeneous fuel distribution inside the spray cloud.

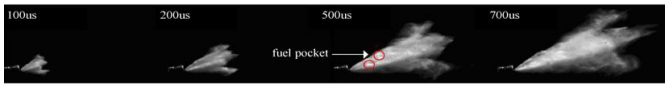

Figure 2: Experimental detection of the GDI spray evolution. P_{inj}=20 MPa and m_{inj}=50 mg/stroke.

Post-processing the spray pictures, for each considered test configuration the time-evolutions of the spray penetration and cone angle were measured. In particular, both these parameters were measured for the jet disposed orthogonally with the CCD camera axis. Figures 3 and 4 show the influence on penetration and cone angle of the injection pressure for a total injected fuel mass equal to 50 mg/stroke. About the penetration evolution (Figure 3), during the first injection part (time lower than 500 μs) all the profiles show a typical linear trend versus time. Only after 500 μs from the hydraulic SOI, the different droplet momentum (linked to the different injection pressure) started to play a role against the gas resistance effect on the droplets. About the single spray cone angle, Figure 4 shows how this parameter was only slightly influenced by the injection pressure. In particular, fixing the total mass injected at 50 mg/stroke, for all the three considered injection pressures the single spray cone angle converged asymptotically to a value near 12°.

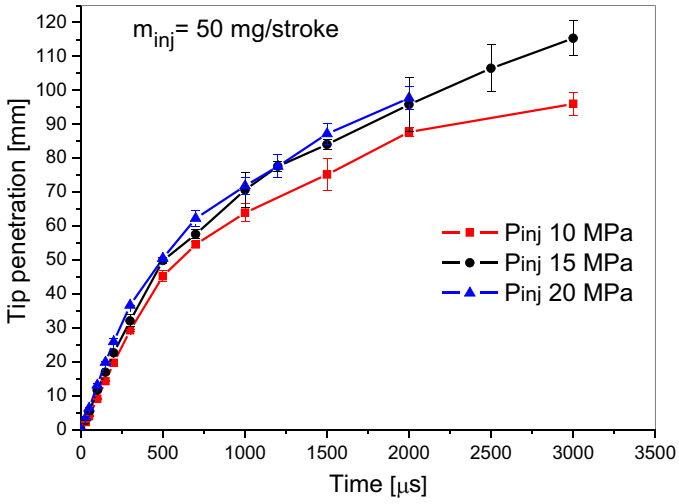

Figure 3: Spray tip penetration at 10, 15 and 20 MPa of injection pressure. Fuel mass injected: 50 mg/stroke.

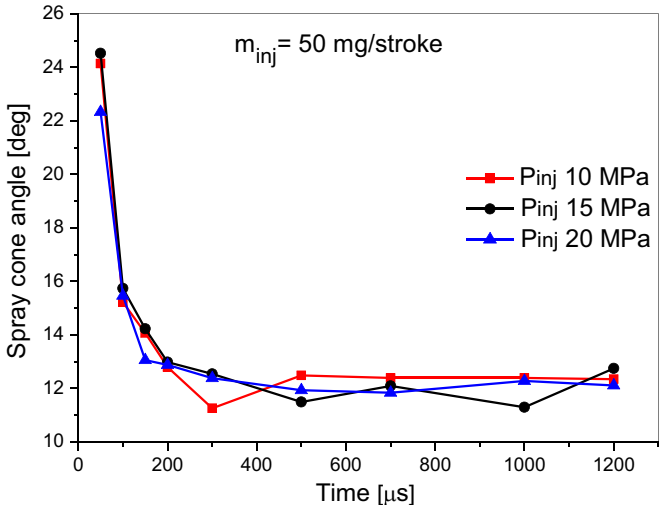

Figure 4: Cone angle at 10, 15 and 20 MPa of injection pressure. Fuel mass injected: 50 mg/stroke.

Image sequences of the spray evolution, taken simultaneously by two synchronized cameras orthogonally disposed, are reported in Figure 5 for the condition 20 MPa of injection pressure, 50 mg/stroke of delivered fuel and at atmospheric backpressure of the gas in the vessel. The frontal view of the sprays (top of the strips) highlights the evolution of the jet plumes coming out of the paper (the axis of the nozzle is parallel to the optical axis of the CCD lens). It shows an independent growth of the sprays up to about 200 μs from the SOI. The propagation of the jets are well defined indicating the fuel distribution inside the vessel. This regularity appears destroyed for the images at 500 and 700 μs where the interference between the single jets appears evident and the single jet evolution cannot be longer followed. Here the fuel figure has to be considered as a single, large and composite spray.

The lateral spray evolution view allows to distinguish the origin of the single jets close to the nozzle exit. Four single, well confined sprays appear in the foreground of the CCD view plane while two sprays are in the background and hidden from view.

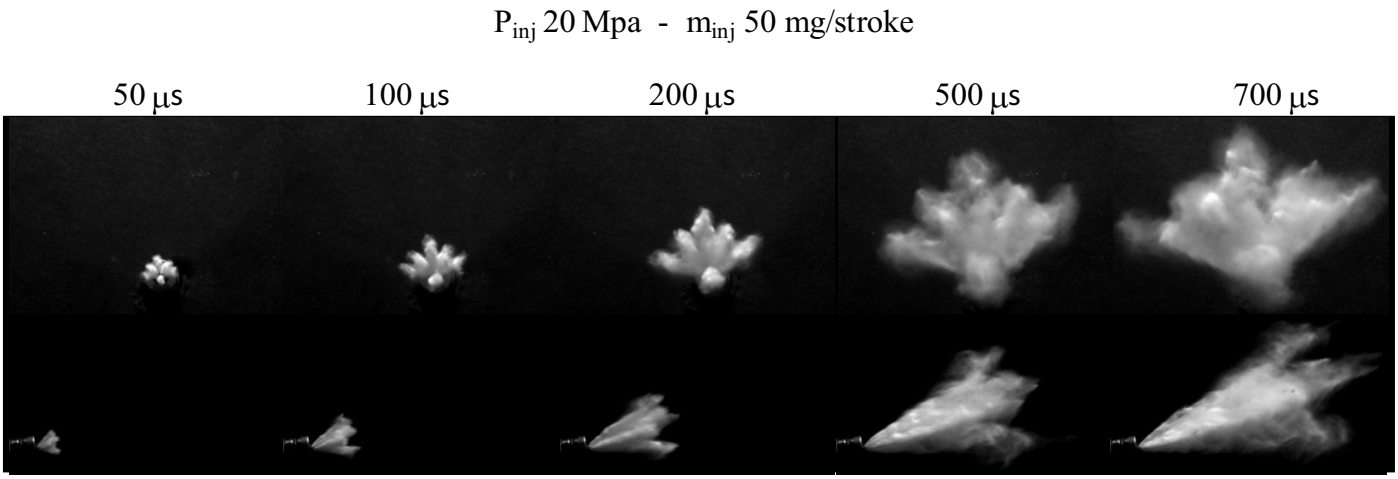

Figure 5: Spray evolution sequences at the indicated conditions taken frontally (top) and laterally (bottom)

As previously introduced, also the wall film generation and evolution was experimentally produced. To this end, the impact between the jets from the GDI injector and a flat plate was carried out. It was made for the working condition characterized by a P_{inj} of 20 MPa and m_{inj} of 50 mg/stroke. Figure 6 presents the picture sequence captured during the experimental test. As showed, the spray advanced freely into the vessel until 400 μs from the hydraulic SOI instant. Obviously, with respect to the same injection configuration previously tested without the plate, no changes were detected about the overall spray behavior until this instant. After 400 μs from hydraulic SOI, the first jet reached the plate surface starting to spread on it. At later time (800 μs) all the jets reached the plate and a uniform layer of fuel compensated the interspaces between the jets. At longest time (1400 μs), the different spray directions, therefore the different rebounding angles, produced a lateral evolution of the film. In particular, a compact fuel film having a uniform height was generated on the right side on the plate while on the left side of the plate the wall film was more curled and higher than on the right side (Figure 6). At the end of the injection process all the fuel was distributed laterally on the flat plate.

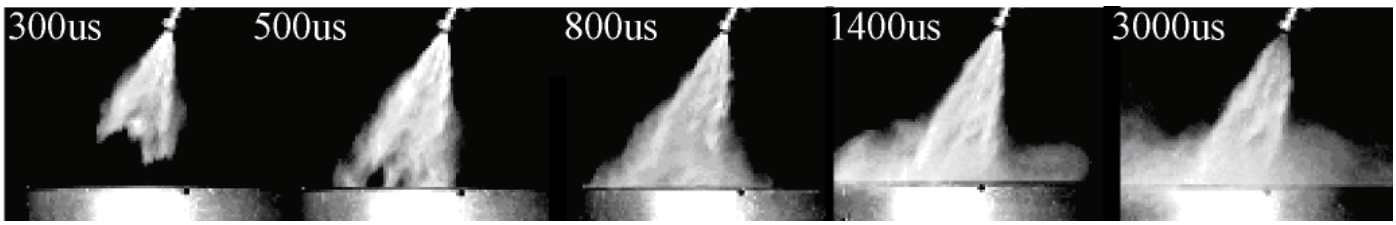

Figure 6: Evolution of the spray impact on the flat plane. P_{inj}=20 MPa and m_{inj}=50 mg/stroke.

CFD Simulations

Table 2 summarizes the injection operating conditions chosen to validate the CFD methodology previously presented. These cases were chosen because both the injection pressure range and the amount of injected fuel mass were typical of multi-hole atomizers usually adopted for GDI engines. Spray computations were subdivided into three steps. To test the proposed atomization model, the spray emerging from a single injector hole was firstly simulated. Then, the complete injector configuration, including all the six sprays, was taken into account to evaluate the effects of the collision model when interactions between multiple jets were present. Finally, experiments of impinging spray on a flat plate were used to validate the liquid film and droplet-wall interaction models. For all the simulations, the gasoline fuel was modeled using the iso-octane liquid properties and droplets were injected according to the experimental mass flow rate profiles. The standard *k-ε* model was used for turbulence.

Table 2: Simulated operating conditions.

	Injection pressure [MPa]	Injected fuel mass [mg/str]	Injection duration [μs]
1	10	20	1450
2	15	50	2900
3	20	50	2600

The single spray simulations were performed considering the same jet chosen as reference during the experimental campaign. As computational domain, a box with 20 x 20 x 120 mm size was used and it was filled with air at atmospheric pressure and ambient temperature (300 K, 1 bar). The injector tip was placed on the top of the test rig. The computational volume was discretized by a spray-oriented grid having an initial size of 4 mm. During the simulation, the Adaptive Local Mesh Refinement technique was adopted to guarantee a good level of convergence to the simulation. In particular, two refinement levels were used, corresponding to a minimum mesh size of 1 mm. The chosen minimum size represents a good compromise between the CPU time required and the results accuracy. It is important to point out that, when the ALMR method is used in spray simulation, the grid is refined only where the spray evolves. As a consequence, also the computed velocity field in that region is better predicted.

To evaluate the performance of the simulation methodology, the first parameter which was compared to experimental data was the spray penetration. The Figure 7 illustrates that the proposed model is able to reproduce the spray penetration dependency on the injection pressure even if a slight overestimation exists until 500 μs after the hydraulic start of injection. However, the overall behavior of the proposed approach could be considered rather satisfactory and for this reason it was employed in the remainder of the simulations where all the six sprays were taken into account.

The computational domain used to simulate the complete injector configuration consisted in a cubic box of 120 mm size and the collision model was activated. Adaptive Local Mesh Refinement was used also in this case, but it was not possible to keep the mesh spray-oriented because of the different spray patterns. This generally happens also in CFD simulations of GDI engines where unstructured meshes are generally adopted to accommodate complex geometry features like piston bowl, canted valves and cylinder head. Figure 8 shows the comparison between experimental and numerical evolution of the full spray for an injection pressure of 20 MPa (the Lagrangian particles were scaled according to their diameter values). Also in this case, in comparison to the experimental evidence, the spray shape, cone angle and penetration were rather well predicted. The effect of the collision model on the spray evolution was detected in terms of fuel cluster generation along the main spray axis. This aspect strongly influences the spray atomization process and probably the fuel-air mixing process as well. Hence, collision has to be taken into account when the evolution of multiple sprays have to be simulated in GDI engines.

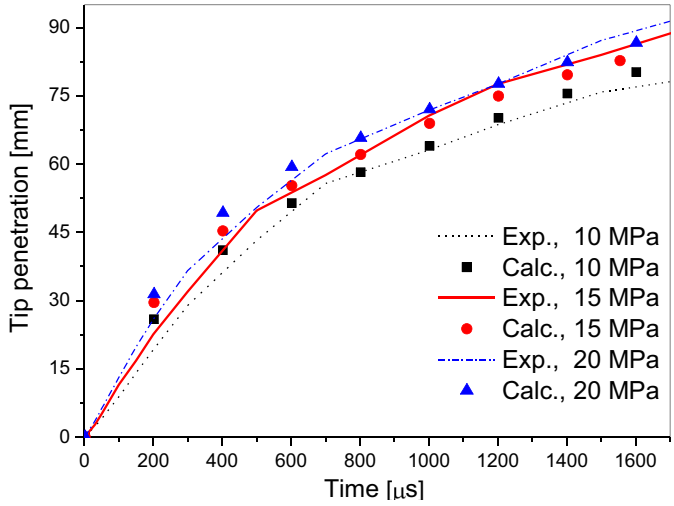

Figure 7: Comparison between computed and experimental spray penetrations as a function of the injection pressure.

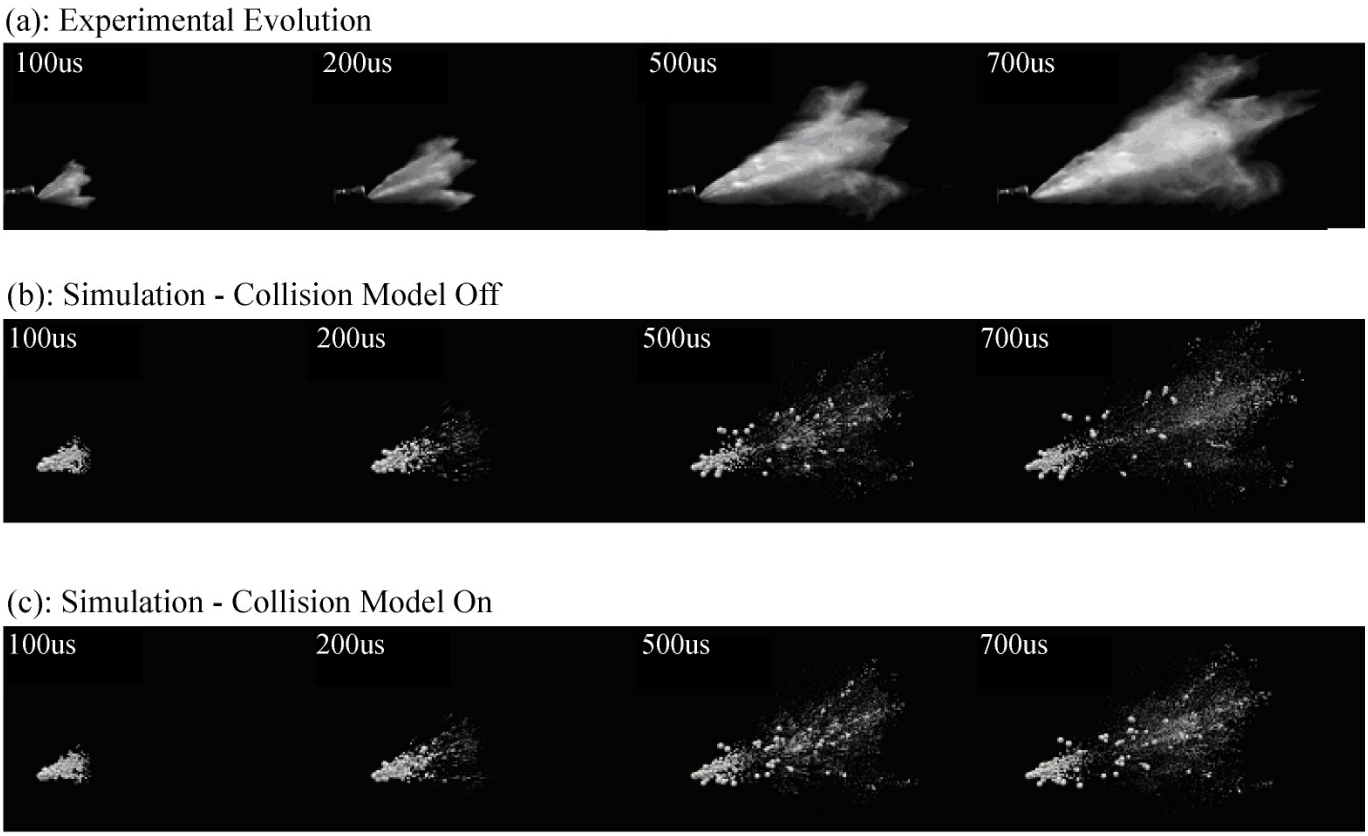

Figure 8: (a) Experimental data of spray evolution at injection pressure of 20 MPa (b) Computed spray evolution without the collision model; (c) Computed spray evolution including the effects of collision and coalescence.

Once a suitable set of spray sub-models was identified to describe fuel atomization and breakup in GDI engines, CFD calculations were performed to verify the droplet-wall interaction and liquid film models. As for experiments, a flat plate was introduced into the computational domain at a distance of 40 mm from the injector tip. The plate was disposed perpendicularly to the jet chosen as reference. For consistence to the experiments, an injection pressure of 20 MPa was chosen.

The computed spray distribution, in combination with the liquid film thickness and velocity field are shown in Figure 9 for different times after the start of injection. The liquid film expands in three different directions that are strictly related to the injector spray patterns. These kind of investigations can be very useful to improve both the injector and the piston bowl design.

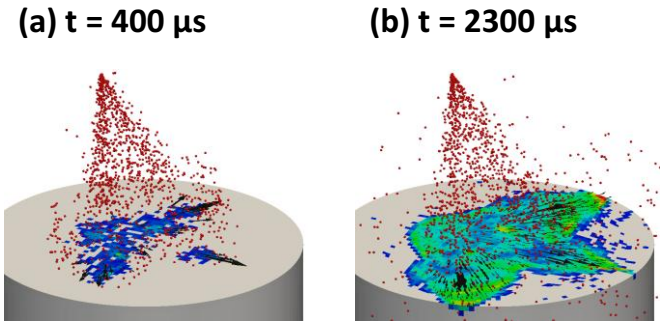

Figure 9: Computed evolution of liquid film thickness and velocity field at 400 and 2300 µs after the start of injection. Liquid film thickness range 0 (blue) to 0.1 mm (red).

In Figure 10, the computed spray evolution is compared to experimental data at impinging conditions. According to the proposed model, impingement starts 300 µs after SOI, which was 100 µs in advance with respect to the measurements. This discrepancy was due to the overestimation of spray penetration, as illustrated in Figure 7. Once impingement was established, the predicted shape of the spray cloud was in rather good agreement with experimental data: two curls were formed on the left and right sides and the first one propagates faster (see Figure 10). The model also seemed to reproduce correctly the maximum value of the wall spray height. For a further validation of the proposed wall-film model, more experiments are required to verify the validity of the droplet-wall interaction model and the influence of the Leidenfrost effects that has to be taken into account because of the high temperatures of the cylinder walls.

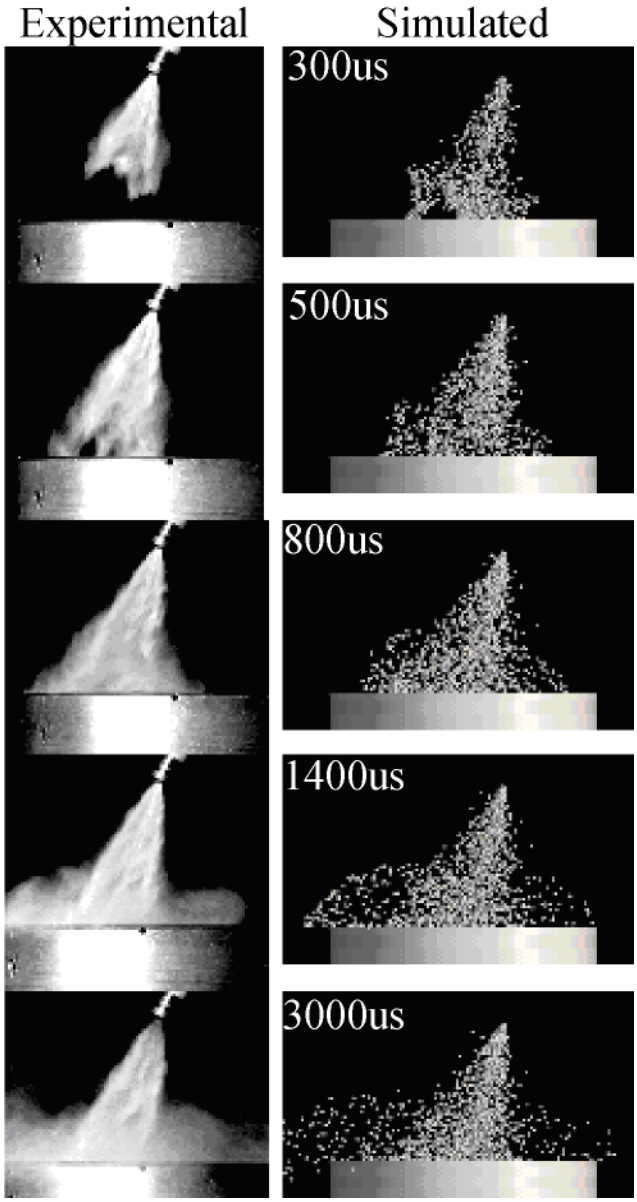

Figure 10: Comparison between computed and experimental spray evolution at impinging conditions.

CONCLUSIONS

Experiments and simulations were carried out to investigate the behavior of non-evaporating sprays emerging from a multi-hole injector designed for GDI applications. Purpose of this work was to define a suitable CFD methodology to model the fuel-air mixing process in GDI engines and, at the same time, to identify a set of experiments and operating conditions that can be helpful to improve the existing numerical models. The proposed CFD approach accounts for the main processes governing cavitation inside the nozzle, fuel atomization, droplet breakup, collision/coalescence and interaction with the walls. Experimental data of spray penetration, cone angle together with optical images were available for validation. The global evolution of the spray was investigated by the imaging technique applying the digital processing of images, acquired by a synchronized CCD camera. The main experimental results can be summarized as:

- The plumes of the single jets develop independent each other for different time from the SOI depending on the injection conditions. At 20 MPa the jets start to interfere at 500 μs,
- Fuel pockets appear in the jet images indicating a non-homogeneous distribution of the fuel inside the spray,
- The injection pressure strongly influences the penetration while total amount of delivered fuel produce negligible effects,
- About the spray cone angle, slight effects come from the injection pressure and no variations are due to the injected fuel amount.

Computed results correctly reproduce the experimental trends in terms of spray penetration dependency on the injection pressure and droplet distribution including also impinging conditions. Despite a rather satisfactory agreement was obtained, calculations revealed the need to perform further experiments in future work to better clarify how spray evolution is influenced by the following phenomena:

- Cavitation inside the nozzle,
- Influence of collision and coalescence on droplet diameter and evaporation rate,
- Effects of the different impinging regimes on the liquid film formation and evolution,
- Influence of the Leidenfrost effect on the liquid film evolution.

To this end, new experimental conditions are being investigated by the authors. In particular, a Phase Doppler Anemometry (PDA) system is now available to measure the droplet size and velocity at different distances from the injector.

NOMENCLATURE

D_d: droplet diameter.
d_0: droplet diameter before impingement.
L_{nozz}: injector nozzle length.
L_{t0}: liquid turbulent length scale at the nozzle exit.
V_{cell}: cell volume.
V_p: droplet velocity at impinging conditions.
We: droplet impact Weber number.
We_s: Weber number defining splashing conditions.
Y_{l+g}: total fuel mass fraction in each computational cell.
Y_f: fuel vapor mass fraction in a computational cell.
α: spray cone angle.
ε_{d0}: turbulent kinetic energy dissipation rate at the nozzle exit.
μ: liquid dynamic viscosity.
Ω: growth rate.
ρ: gas density.
σ: liquid surface tension.
τ_{t0}: liquid turbulent time-scale at the nozzle exit.
$K_c, K_\varepsilon, B_1, C_1, C_3$: model tuning constants.

REFERENCES

[1] Zhao, F. Q., and Lai M., "A Review of Mixture Preparation and Combustion Control for Spark-Ignited, Direct-Injection Gasoline Engines," SAE Technical Paper 970627, 1997.

[2] Shahed, S. M., and Bauer K. H., "Parametric Studies of the Impact of Turbocharging on Gasoline Engine Downsizing," SAE Int. J. Engines (2):1347-1358, 2009.

[3] Rivera, E. A., Mastro, N., Zizelman, J., Kirwan, J., Ooyama, R., "Development of Injector for the Direct Injection Homogeneous Market using Design for Six Sigma, " SAE Technical Paper 2010-01-0594, 2010.

[4] Adomeit, P., Weinowski, R., Ewald, J., Brunn, A., Kleeberg, H., Tomazic, D., Pischinger, S., Jakob, M., "A New Approach for Optimization of Mixture Formation on Gasoline DI Engines," SAE Technical Paper 2010-01-0591, 2010.

[5] Matsumoto, A., Moore, W, Lai, M., Zheng, Y., Foster, M., Xie, X., Yen, D., Confer, K., Hopkins, E., "Spray Characterization of Ethanol Gasoline Blends and Comparison to a CFD Model for a Gasoline Direct Injector," SAE Technical Paper 2010-01-0601, 2010.

[6] Nauwerck, A., Pfeil, J., Velji, A., Spicher, U., Richter, B., "A Basic Experimental Study of Gasoline Direct Injection at Significantly High Injection Pressures", SAE Technical Paper 2005-01-0098, 2005.

[7] Abart, M., Schmidt, S., Schoegl, O., Trattner, A., Kirchberger, R., Eichlseder, H., Jajcevic, D., "Basic Investigations on the Prediction of Spray-Wall and Spray-Fluid Interaction for a GDI Combustion Process", SAE Technical Paper 2010-32-0030, 2010.

[8] Nordin N., "Complex Chemistry Modeling of Diesel Spray Combustion," PhD thesis, Chalmers University of Technology, Department of Thermo Fluid Dynamics, Goteborg, 2001.

[9] Lucchini T, D'Errico G., Brusiani F., Bianchi G. M., "A Finite-Element Based Mesh Motion Technique for Internal Combustion Engine Simulations," presented at COMODIA 2008, Sapporo, Japan, July 27-31, 2008.

[10] Montenegro G., Onorati A., Piscaglia F., D'Errico G., " Integrated 1D-MultiD Fluid Dynamic Models for the Simulation of I.C.E. Intake and Exhaust Systems," SAE Technical Paper 2007-01-0495, 2007.

[11] OpenFOAM, "The Open-source CFD toolbox," http://www.openfoam.org/, September 2010.

[12] Lucchini, T., Ettorre, D., D'Errico, G., Brusiani, F., Bianchi, G., Montanaro, A., Allocca, L., "Experimental and Numerical Investigation of High-Pressure Diesel Sprays with Multiple Injections at Engine Conditions", SAE Technical Paper 2010-01-0179, 2010.

[13] Lucchini, T., D'Errico, G., Brusiani, F., Bianchi G. M., Tukovic Z.,Jasak, H. "Multi-dimensional modeling of the air/fuel mixture formation process in a PFI engine for motorcycle applications," SAE Technical Paper 2009-24-0015, 2009.

[14] Bosch, W. "The Fuel Rate Indicator: a New Measuring Instrument for Display of the Characteristics of Individual Injection", SAE Paper 6607496, 1966

[15] Wallace: I. " Injection Rate Gauge: Pass Off Information and User Instructions" - Fuel & Engine Management Systems, Graz - December 2002

[16] Alfuso, S., Allocca, L., Caputo, G., Corcione, F.E., Montanaro, A., Valentino G.,: "Experimental Investigation of a Spray from a Multi-jet Common Rail Injection System for Small Engines" SAE_NA 2005-24-9

[17] Huh, K. Y., Gosman, A. D., "A Phenomenological Model of Diesel Spray Atomization," Proceedings of the International Conference on Multiphase Flows, September 24-27, Tsukuba, Japan, 1991.

[18] Bianchi, G. M., Pelloni, P., "Modeling the Diesel Fuel Spray Breakup by Using a Hybrid Model," SAE Technical Paper 1999-01-0226, 1999.

[19] Reitz, R. D. "Modeling Atomization Processes in High-Pressure Vaporizing Sprays," Atomization and Spray Technology (3): 309–33, 1987.

[20] Reitz, R.D., Bracco, F. V., "Mechanisms of Breakup of Round Liquid Jets," In Encyclopedia of Fluid Mechanics, Gulf Pub, (3):233–249, 1986.

[21] Brusiani, F., Falfari, S., Forte, C., "The Role of Cavitation inside High Pressure GDI", ATI Technical Paper ATI09-11-009, 2009.

[22] Qian J., Law K., "Regimes of Coalescence and Separation in Droplet Collision," J. Fluid Mech (331):59–80, 1997.

[23] Stanton, D., Lippert, A., Reitz, R. D., Rutland, C.J., "Influence of Spray-Wall Interaction and Fuel Films on Cold Starting in Direct Injection Diesel Engines," SAE Technical Paper 982584, 1998.

[24] Kolpakov, A. V. et al., "Calculation of the Rebound Condition for Colliding Drops of Sharply Different Sizes," Kollodn. Zh. (47), 1985.

[25] Stanton D., and Rutland, C.J., "Modeling fuel film formation and wall interaction in diesel engines," SAE Technical Paper 960628, 1996.

[26] Yarin, A. L., and Weiss, D. A., "Impact of Drops on Solid Surfaces: Self-Similar Capillary Waves, and Splashing as a new Type of Kinematic Discontinuity,". Journal of Fluid Mechanics (283), 1995.

[27] Senecal, P. K., Richards, K. J., Pomraning, E., Yang, T., Dai, M. Z., McDavid, R. M., Patterson, M. A., Hou, S., Shethaji, T., "A New Parallel Cut-Cell Cartesian CFD Code for Rapid Grid Generation Applied to In-Cylinder Diesel Engine Simulations," SAE Technical Paper 2007-01-0159, 2007.

[28] Lippert A. M., Chang S., Are S., Schmidt D.P, "Mesh Indipendence and Adaptive Mesh Refinement For Advanced Engine Spray Simulations," SAE Technical Paper 2005-01-0207, 2005.

[29] Jasak H., "Error Analysis and estimation for the finite volume method with applications to fluid flows," Ph.D. thesis, Imperial College of Science, Technology and Medicine, London, 1996.

[30] Lucchini, T., Ettorre, D., D'Errico, G., Ferrari, G.," Numerical Investigation of Non-Reacting and Reacting Diesel Sprays in Constant-Volume Vessels," SAE Int. J. Fuel and Lubr. (2):966-975, 2009.